Shock Waves (2009) 19:1–10
DOI 10.1007/s00193-008-0178-2

ORIGINAL ARTICLE

Fundamentals of rotating detonations

Manabu Hishida · Toshi Fujiwara · Piotr Wolanski

Received: 31 March 2008 / Revised: 13 October 2008 / Accepted: 4 November 2008 / Published online: 10 February 2009

Abstract A rotating detonation propagating at nearly Chapman–Jouguet velocity is numerically stabilized on a two-dimensional simple chemistry flow model. Under purely axial injection of a combustible mixture from the head end of a toroidal section of coaxial cylinders, the rotating detonation is proven to give no average angular momentum at any cross section, giving an axial flow. The detonation wavelet connected with an oblique shock wave ensuing to the downstream has a feature of unconfined detonation, causing a deficit in its propagation velocity. Due to Kelvin–Helmholtz instability existing on the interface of an injected combustible, unburnt gas pockets are formed to enter the junction between the detonation and oblique shock waves, generating strong explosions propagating to both directions. Calculated specific impulse is as high as 4,700 s.

Keywords Rotating detonation · Unconfined detonation · Detonation wavelet · Kelvin–Helmholtz instability · Unburnt pocket · Standing detonation

PACS 47.40.Rs

1 Description of problem

During the present CFD work aiming at "Rotating Detonation Engine" which is based on a detonation wave rotating in a toroidal area in a coaxial cylinder, as shown in Fig. 1a, a number of interesting physics has been discovered on the rotating detonation wave. The rotating detonation that is steadily propagating azimuthally is not propagating forward into the axial direction because it is blocked by the existence of the head wall, even if the incoming axial velocity of fuel-gas mixture is much less than the Chapman–Jouguet velocity of detonation. Such rotating detonations have been experimentally observed and analyzed since 1957 by Nicholls, Voitsekhovskii, ensuing Russian workers and Wolanski [1–6], with a long intermission during 1960's–1990's. Nevertheless experimental observations have essentially been limited just to the detection of detonation radiation due to the three-dimensionality of rotating detonations. Only very limited research has been done theoretically, which is always directed to application to aerospace thrusters [7]. In contrast, the present CFD work has revealed a number of surprising physical aspects that exist only in rotating detonations. Here we show (1) a character of detonation-shock combined wave or unconfined detonation [8–10] causing a deficit in rotating velocity, (2) the existence of Kelvin–Helmholtz instability on combustible interface with relevant generation and explosion of unburnt gas pocket, (3) a steady aspect as extension of standing detonation for subsonic injection of combustibles, and (4) a high specific impulse applicable to various engineering fields. Such interesting phenomena may be helpful to understand detonations even in supernova physics.

2 Modeling and numerical method

The rotating detonation engine that is analyzed by the present study is shown in Fig. 1a. A detonation wave is rotating azimuthally in a toroidal channel between two coaxial cylinders, while a combustible gas is axially injected from the head end and the burnt gas flows out from the downstream exit. This concept of flow can be justified because it has already been established by a group of experimental studies [4–6]. The

Communicated by F. Zhang.

M. Hishida · T. Fujiwara (✉)
Nagoya University, Nagoya 464-8603, Japan
e-mail: fujiwaratos35@ybb.ne.jp

P. Wolanski
Warsaw University of Technology, 00661 Warsaw, Poland

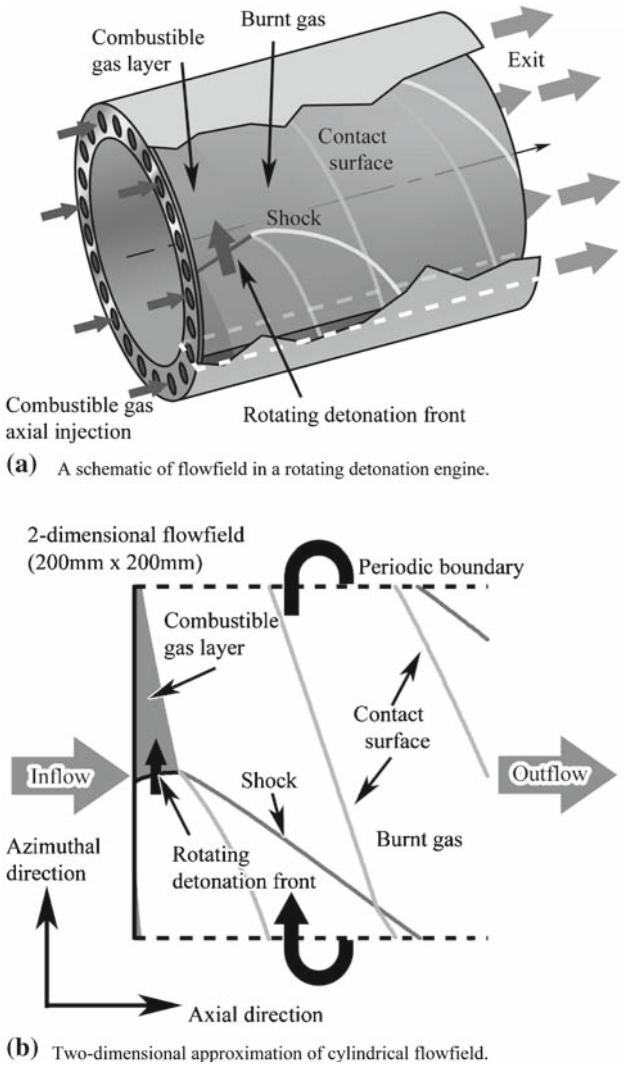

Fig. 1 A rotating detonation engine and its two-dimensional CFD model

primary purpose of the present study is (1) to run a stably propagating detonation, (2) to describe interesting physical phenomena and (3) to discuss whether the rotating detonation engine is realistic in application to thrusters or power generators.

Assuming that the distance between the two coaxial cylinders is much smaller than their diameters and that the diameter is not too small to create a strong centrifugal force to the flow, the flowfield can be approximated as a plane two-dimensional area 200 mm × 200 mm, as shown in Fig. 1b. Except that the upstream and downstream conditions are identical to the cylindrical flow, the upper and lower sides are connected by periodic boundary conditions.

2.1 Boundary conditions

Modeling of the boundary conditions is one of the most important issues in the present analysis. In view of the existing experiments, the boundary conditions are set to be as simple as possible to make the analysis easy, without losing general characters and holding consistency with Euler Equations and a part of experimental conditions.

(a) The inflow condition is set up as follows: At $t = 0$, the reservoir pressure and temperature are adjusted to give a specified Mach number in the fictitious uniform region (the pressure 0.2 MPa, the temperature 300 K) in the quiescent toroidal area, after choking and subsequent isentropic expansion prevail. For this adjusted reservoir condition, at $t > 0$ after a real rotating detonation has started running, the injection velocity is decided at each azimuthal location by its local pressure, depending upon where the place is along the azimuthal axis. (i) Immediately behind the detonation front, the pressure is usually higher than the reservoir pressure; in such circumstances the injection velocity is assumed zero. (ii) Far from the detonation front, the pressure could be lower than the choking value; then the injection velocity is given by the choking condition. (iii) In the intermediate region where the pressure is between the reservoir and choking ones, the injection velocity is calculated by the isentropic expansion from the reservoir condition.

(b) The reservoir condition: The reservoir condition is assumed unaffected by the downstream condition, staying constant throughout the analysis. In reality a reverse flow into the reservoir can happen when the flowfield pressure exceeds the reservoir one, which certainly necessitates taking account of modeling a large size of reservoir area. In the present modeling, however, such phenomenon is not included to simplify the analysis.

(c) The headwall temperature: Due to constant exposure to a hot burnt gas behind the detonation front, the headwall temperature can be high, supplying a heated unburnt mixture flow even if it is cooled to some extent by cold fuel from the reservoir. This phenomenon is not considered in order to be consistent with the use of Euler Equations.

(d) Thus, the entire flowfield is initially filled with an Ar-diluted oxyhydrogen mixture ($2H_2 + O_2 + 7Ar$) at $P_1 = 0.2$ MPa and $T_1 = 300$ K, except near the head wall region where an azimuthally propagating C–J detonation wavelet is artificially placed assuming its structure identical to a 1-dimensional detonation. The headwall boundary is considered nonslip, adiabatic and non-catalytic.

(e) At exit plane: The specific pressure boundary condition is used where no other constraints are imposed on the flow properties because the outgoing flow is known to be always supersonic for a steady rotating detonation.

2.2 Governing equations

The flowfield is governed by the two-dimensional Euler equations, which consist partly of the mass-conservation equations for the progress variable α corresponding to the induction reaction and the variable β corresponding to the exothermic reaction:

$$\frac{\partial U}{\partial t}+\frac{\partial E}{\partial x}+\frac{\partial F}{\partial y}=S, \tag{1}$$

where we have

$$U=\begin{pmatrix}\rho\\ \rho u\\ \rho v\\ e\\ \rho\beta\\ \rho\alpha\end{pmatrix},\quad E=\begin{pmatrix}\rho u\\ \rho u^2+p\\ \rho uv\\ (e+p)u\\ \rho\beta u\\ \rho\alpha u\end{pmatrix},$$
$$F=\begin{pmatrix}\rho v\\ \rho uv\\ \rho v^2+p\\ (e+p)v\\ \rho\beta v\\ \rho\alpha v\end{pmatrix},\quad S=\begin{pmatrix}0\\ 0\\ 0\\ 0\\ \rho\omega_\beta\\ \rho\omega_\alpha\end{pmatrix}. \tag{2}$$

The equation of state for a perfect gas is assumed and the pressure is defined as

$$p=(\gamma-1)\left\{e-\rho\beta Q-\frac{1}{2}\rho(u^2+v^2)\right\} \tag{3}$$

where γ and Q are the specific heat ratio (1.4 in this model) and the exothermicity.

As chemistry the modified Korobeinikov–Levin model is utilized, giving the source terms for the two progress variables α and β

$$\omega_\alpha\equiv\frac{\mathrm{d}\alpha}{\mathrm{d}t}=\frac{1}{\tau_{\mathrm{ind}}}=-k_1\rho\exp\left(-\frac{E_1}{\mathrm{RT}}\right) \tag{4}$$

$$\omega_\beta\equiv\frac{\mathrm{d}\beta}{\mathrm{d}t}=\begin{cases}0 & (\alpha>0)\\ -k_2p^2\left\{\beta^2\exp\left(-\frac{E_2}{\mathrm{RT}}\right)-(1-\beta)^2\exp\left(-\frac{E_2+Q}{\mathrm{RT}}\right)\right\} & (\alpha\le 0)\end{cases} \tag{5}$$

where τ_{ind} denotes the induction time. The constants in (4) and (5) are selected to agree with Oran's elementary reaction model with regard to the induction time and temperature profile.

2.3 Numerical method

The HLLE scheme with MUSCL method, in which Van Albada limiter is applied to realize the TVD condition, is used to evaluate the numerical flux of advection terms in (1). In order to solve unsteady problems with high resolution, the four-step Runge-Kutta time integration is used.

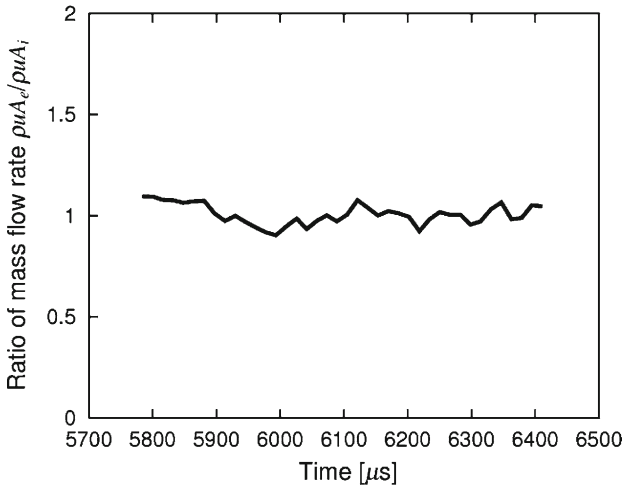

Fig. 2 Temporal variation of mass flow ratio between exit and injection planes

3 Computational resolution and conservation laws

The utilized grid size 100 μm for our Euler analysis is small enough in comparison with the chemical induction distance 250 μm for the Chapman–Jouguet detonation of the present mixture. For a fairly long time in the calculation, a coarse grid size 200 μm is utilized until a stable rotating detonation is established. And then the calculation is suddenly switched to a fine grid 100 μm until again a periodical (fluctuating but nearly steady) motion is reached. The calculated cell size is also found close to the experimental value.

Other important laws had better be checked from the viewpoint of computational resolution and application of the flowfield to thrusters or power generators. The mass conservation law is seen to hold in Fig. 2 which shows the temporal variation of mass flow ratio between injection and exit planes. Although it is fluctuating due to the inherent character of detonation, the ratio is always kept unity, because the flowfield is basically steady. Besides, the angular momentum is considered nearly zero at any circular cross section between the injection wall and exit plane, after a nearly steady flowfield is established. The ratio less than 3 % between density-averaged azimuthal and axial velocities at the exit plane, shown in Fig. 3, confirms the angular momentum conservation, since at the inlet the injected gas has an axial component only. This axial flow character is an important aspect for rotating detonations to be applied to aerospace thrusters.

4 Results and discussion

4.1 Steady rotation

In the present calculation as well as in experiment [6], a rotating detonation can be established after several rotations. A typical experimental result (Fig. 4) gives an extremely

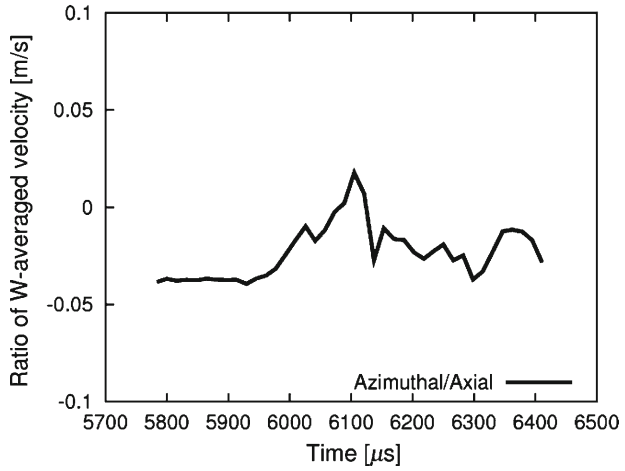

Fig. 3 Temporal variation of ratio between weight (density)-averaged azimuthal and axial velocities at exit plane—order of 3 %

stable rotating detonation propagating in the toroidal area of coaxial cylinders with the diameters 140/150 mm. The detonation keeps rotating several hundred times until the supply gas mixture H_2 + Air runs out. The observed rotating speed 1,410 m/s is substantially lower than its C–J value, caused by numerous experimental reasons including insufficient mixing. Although Fig. 4 is referred to give just qualitative but not quantitative comparisons with Fig. 5, experimentally-observed stable rotations are seen in the calculated result as well (Fig. 5), which gives very stable pressure peaks 3–4 MPa with a nearly repeatable peak-to-peak time interval 132.6 μs. The azimuthal propagation velocity D_{ROT} is given by 200 mm/132.6 μs = 1508.3 m/s. The average value after $t = 6,100\,\mu s$ gives a slightly lower value $D_{ROT} = 1503.5$ m/s. On the other hand, the injection velocity of unburnt gas right in front of rotating detonation is measured as $V_{INJ} = 259.8$ m/s which corresponds to the boundary condition (iii), i.e. the case of isentropic expansion. The vector sum of these two velocities $D = (D_{ROT}^2 + D_{INJ}^2)^{1/2} = 1525.8$ m/s, which is the propagation velocity of our rotating detonation to the direction of outward normal to detonation front. Stable rotation can be seen in Fig. 6 where the averaged pressure and temperature at an injection plane are stabilized after $t = 6,100\,\mu s$ (two rotations after converting to the grid size 100 μm).

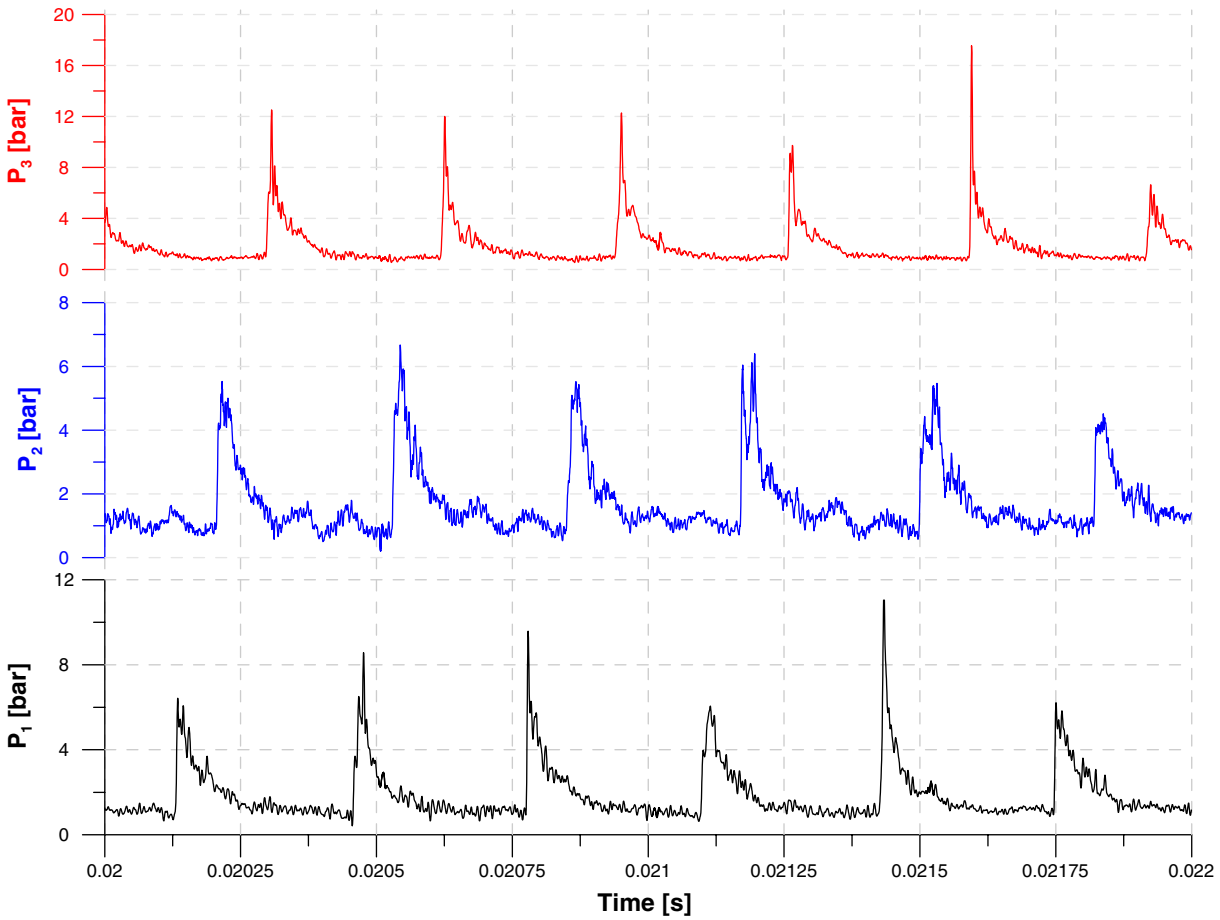

Fig. 4 Experimentally-observed rotating detonation azimuthally propagating in a toroidal part of coaxial cylinders with the diameters $D = 140/150$ mm for a mixture H_2 + stoichiometric air at $p_0 = 0.1$ MPa. Three pressure probes are placed on one cross section where a single rotating detonation propagates, indicating that for several hundred cycles of experimental duration the detonation shows steady rotations

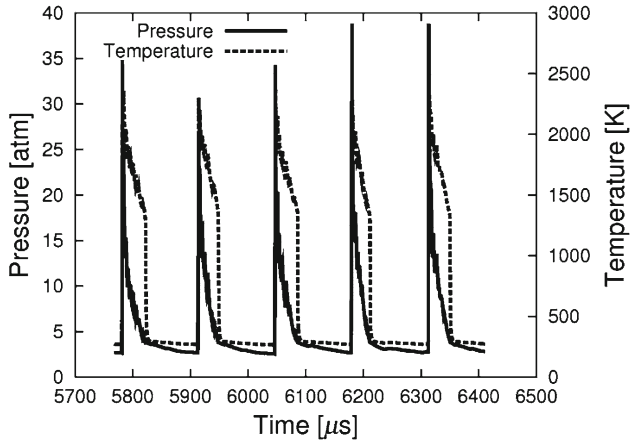

Fig. 5 Temporal variations of pressure and temperature at a location ($z = 0.05$ mm, $\phi = 100$ mm) immediately behind injection wall, indicating a steadily rotating detonation

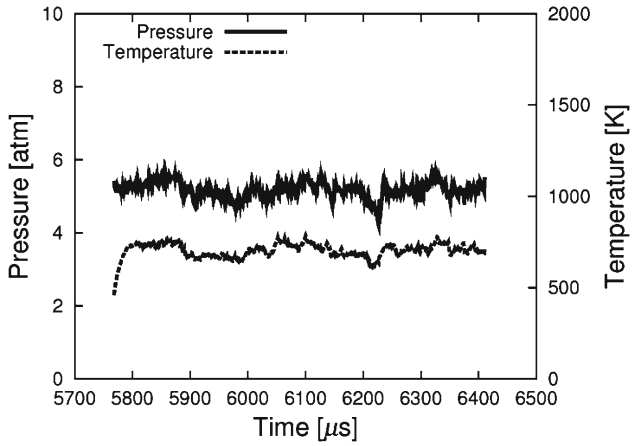

Fig. 6 Temporal variation of pressure and temperature averaged over the cross section immediately behind injection wall (axial location 0.050 mm), indicating convergence to nearly steady rotation

4.2 The overall flowfield

A typical example of the entire flowfield is given by the temperature, pressure and velocity distributions at $t = 6298.5\,\mu$s (Figs. 7, 8, 9), which can visualize the distinctive features of existing physical phenomena. The feature of a rotating detonation wavelet penetrating into an unburnt combustible gas layer is clearly depicted. Because of gas injection from the head wall (see Fig. 1b), the detonation front is inclined to the wall surface, where the propagation velocity normal to the front is $D = 1525.8$ m/s, as given in Sect. 4.1. Although one side of the detonation wavelet touches the head wall, the other side is in soft contact with the burnt gas and is entailing an oblique shock wave which extends to the far downstream. Thus this rotating detonation has a character of unconfined or free detonation which was called "a detonation-shock combined wave" by Fujiwara and Tsuge in [9,10], as is shown by

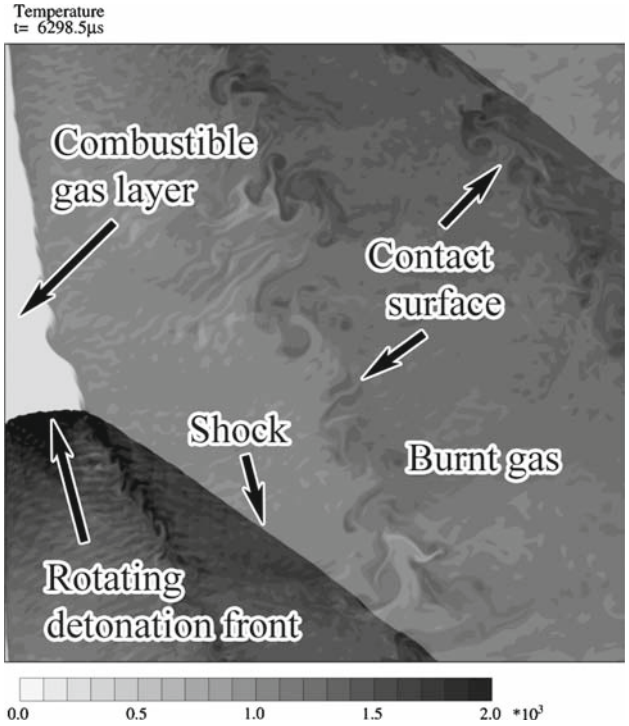

Fig. 7 Temperature distribution in entire flowfield at $t = 6298.5\,\mu$s (during steady rotation)

comparison with Fig. 10. Note also that several triple shocks exist on the surface of rotating detonation, the fingerprint of which can more clearly be seen in the pressure distribution of Fig. 8. The velocity vectors shown in Fig. 9 clearly give the existence of contact discontinuities.

4.3 Unconfined detonation wavelet or detonation-shock combined wave

An unconfined detonation wavelet, shown in Fig. 10, was experimentally discovered by Dabora [8] in 1965. In this unconfined detonation, the downstream portion of reaction zone is located partially behind its sonic plane, causing the propagation velocity slightly lower than the C–J value, as shown in Fig. 11, where the propagation Mach number deficit (the difference from the plane C–J value) is given for O_2–O_3 mixtures of various wavelet widths in two different environments. The velocity deficit from the C–J value 1,591 m/s, i.e. (1,591–1525.8)/1,591 = 4% given in the present calculation can be attributed to this unconfined character of detonation wavelet, since the value is of the same order as in Fig. 11.

Because of the lateral expansion of burnt gas column, the column size (thick or thin, depending on the fuel injection velocity) can affect the stable propagation of rotating detonations. For a very thin column caused by a low fuel injection velocity, for example, the rotating detonation would be unable to exist according to Fig. 11.

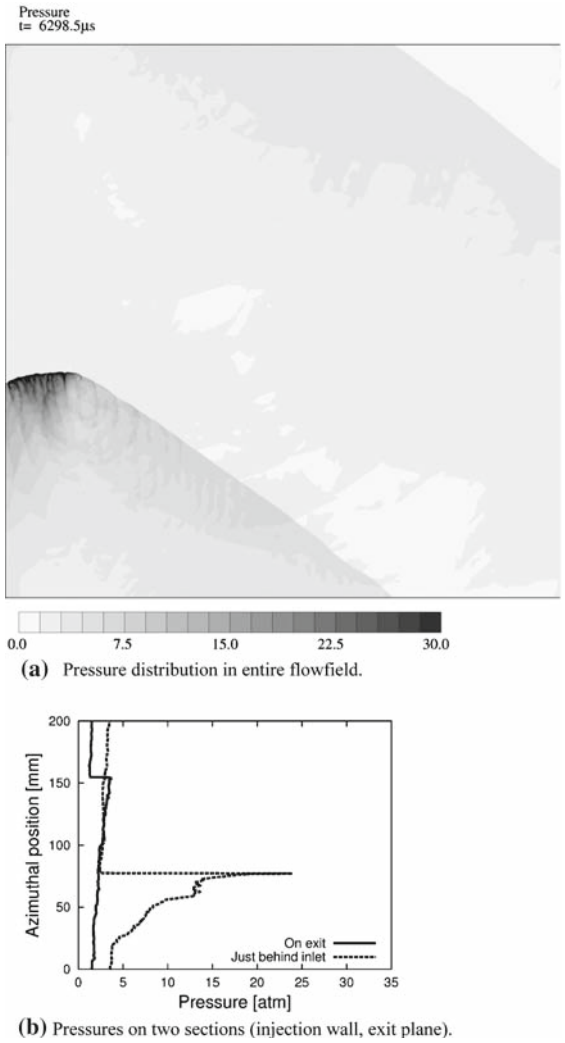

Fig. 8 Pressure distribution at $t = 6298.5\,\mu s$ (during steady rotation)

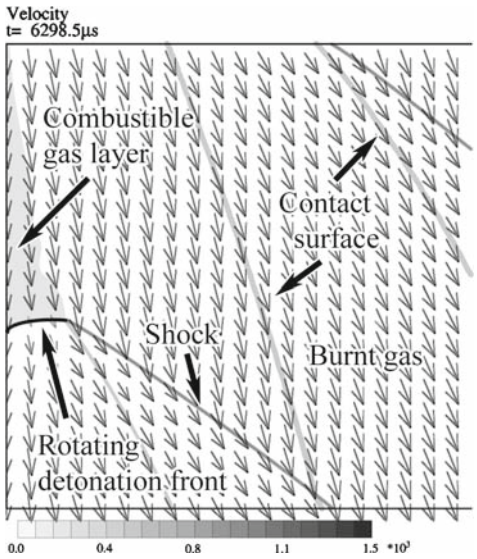

Fig. 9 Velocity distribution in entire flowfield at $t = 6298.5\,\mu s$, viewed from detonation coordinate (during steady rotation)

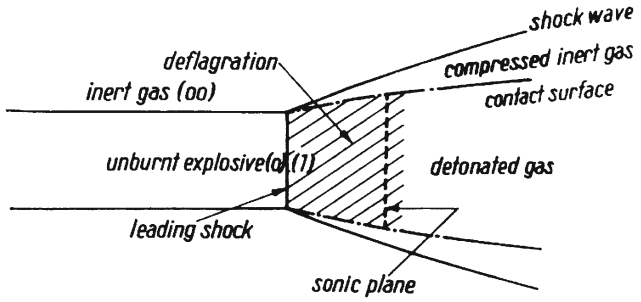

Fig. 10 A sketch of unconfined detonation or detonation-shock combined wave [9,10]

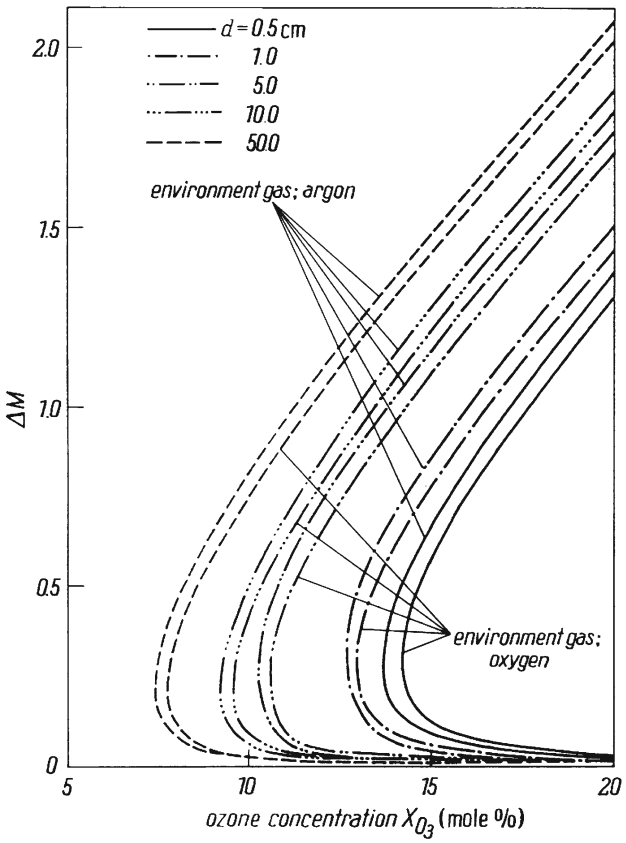

Fig. 11 Propagation velocity deficit in propagation of O_2–O_3 free detonations of various charge diameters in two different environments [9,10]

4.4 Character of standing detonation

Rotating detonations can be considered as an extension of "standing detonation", because it is steadily stabilized by the existence of head wall without propagating in the axial direction. Then the existing concept "standing detonations can exist only for the incoming velocity of combustibles greater than Chapman–Jouguet value" must be altered to "they can exist for any incoming velocities greater than zero". This "superdetonative constraint" has been hampering the appli-

cation of detonation to stable and high-power propulsion devices. Depending upon the combustible gas injection velocity, the length and inclination of rotating detonation wavelet vary, as typically seen in Fig. 7. When the injection velocity is low, the detonation wavelet is short and the wavelet faces nearly to the azimuthal direction. For the increased supply velocities, on the other hand, the wavelet becomes longer with its axial component increasing; for the injection velocity at Chapman–Jouguet value the detonation wave surface becomes completely normal to axis, giving a perfect balance with the incoming flow. Thereafter holds a well-known standing oblique detonation wave over a wedge. Thus it is pointed out that Mother Nature is giving detonations how they can stay at a fixed location for lower injection velocities; in the form of "steady rotation".

4.5 Triple-shock structure, cell size and smoke-foil record

A rotating detonation wavelet is simply an orthodox detonation front containing several triple points, as seen in Figs. 7 and 8. Nevertheless, the cell size 3–3.5 mm is smaller near head wall due to triple shocks colliding with solid wall, while the size 4 mm is larger on the unconfined side because triple shocks have no collision partners just propagating into the ensuing inert oblique shock wave. Such quantitative features are clearly seen on the computed smoke-foil record (Fig. 12).

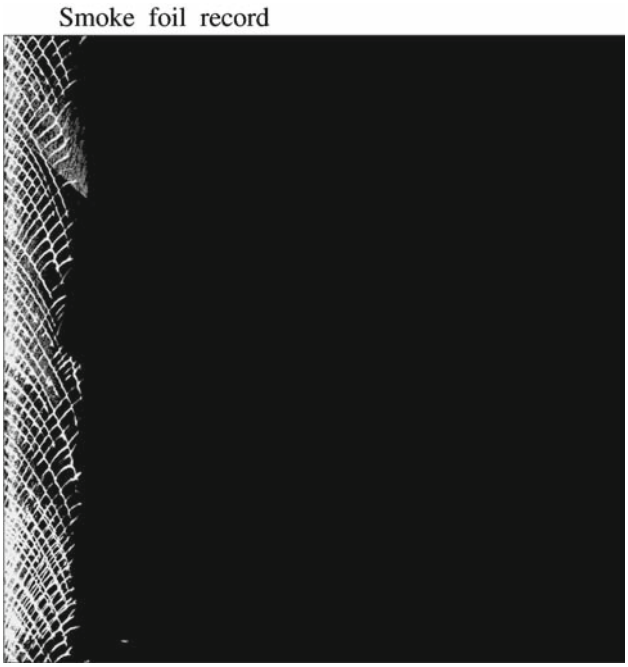

Fig. 12 Smoke-foil record written by triple shocks in rotating detonation after $t = 6{,}250\,\mu s$ (during steady rotation), where white lines are trajectories of pressure higher than 6 MPa during detonation propagation. Cell size is 3–3.5 mm near injection wall, while 4 mm in downstream side

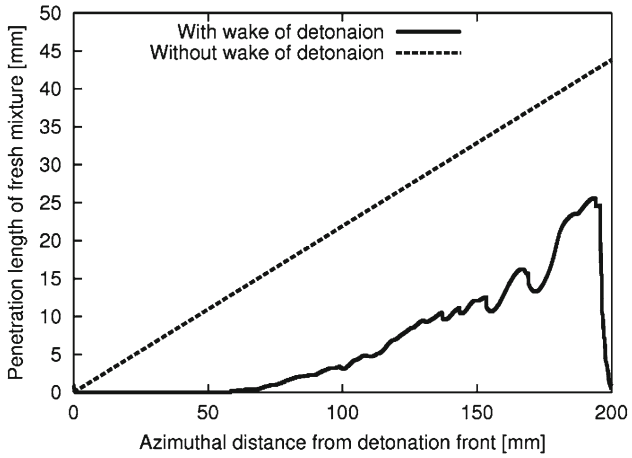

Fig. 13 Structure of unburnt gas at $t = 6298.5\,\mu s$ (during steady rotation). Broken line gives an assumed profile for choking injection where flowfield pressure is low enough to satisfy choking condition between reservoir and flowfield. In reality choking conditions never happen

4.6 Flows at inlet and exit planes

Monitoring the injection of combustible from head wall quantitatively, what kind of boundary condition controls the entire phenomena will be seen. The inert combustible gas layer seen in Fig. 7 is plotted over the entire head wall length 200 mm in Fig. 13; the broken line is shown for comparison purposes giving a fictitious result for injection into a quiescent environment where a choking condition holds. On the other hand, in the real case of rotating detonation, the high pressure field generated by a rotating detonation can give the injection condition either (i), (ii) or (iii), depending upon the local value of pressure. The solid line in Fig. 13 clearly shows that over 60 mm behind the detonation front along the azimuthal axis the local pressure exceeds the reservoir one, giving no injection from the head wall, while in the remaining part a subsonic and isentropic injection is performed. As is also shown in Fig. 8b, the pressure on injection wall always exceeds the choking value 2atm, which justifies the result in Fig. 13.

The temperature distribution on the two planes (injection, exit) in Fig. 14 shows that the temperature at exit plane is 1,100–1,500 K, having non-uniformity caused by the oblique shock wave, while at injection plane the detonation gives the value 1,400–2,000 K.

The velocity distributions on the two planes given in Figs. 15 and 16 show that the axial velocity at exit plane is 600–900 m/s, while the azimuthal one at exit plane stays between −200 and +200 m/s. The temporal behaviors of density-averaged (over exit plane) velocities are shown in Fig. 17, giving the steady and dominant axial flow over the azimuthal one, as a result of angular momentum conservation already discussed by using Fig. 3.

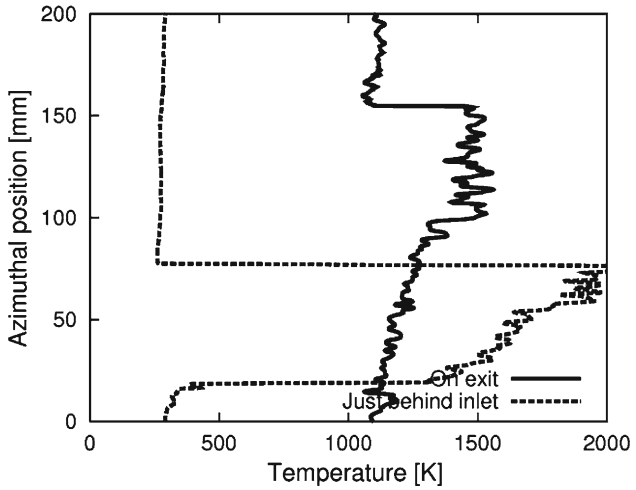

Fig. 14 Temperatures on two sections (injection wall, exit plane) at $t = 6298.5\,\mu s$ (during steady rotation)

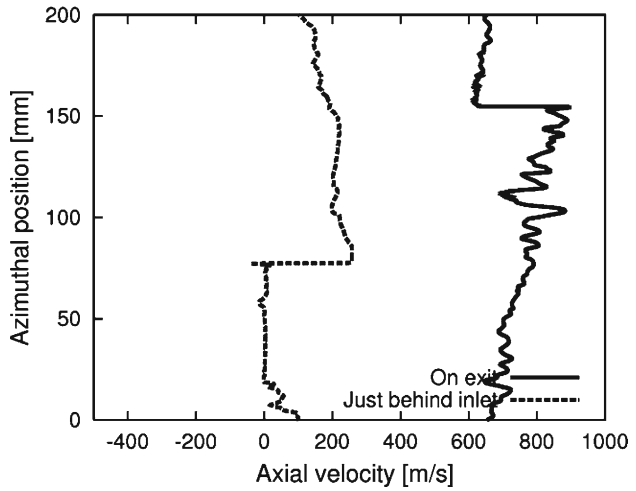

Fig. 15 Axial velocity distributions on two planes (injection wall, exit plane) at $t = 6298.5\,\mu s$ (during steady rotation)

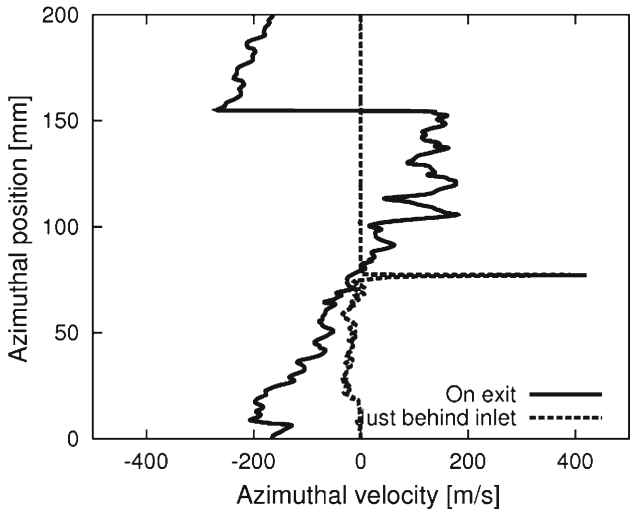

Fig. 16 Azimuthal velocity distributions on two planes (injection wall, exit plane) at $t = 6298.5\,\mu s$ (during steady rotation)

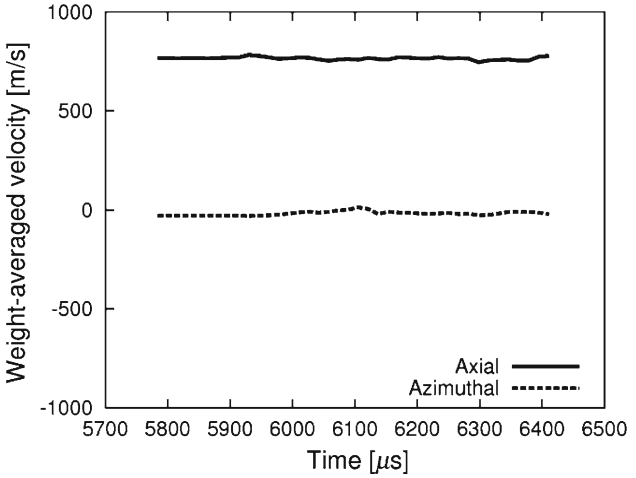

Fig. 17 Temporal variation of two velocities weight/density-averaged over exit plane

4.7 Kelvin–Helmholtz instability on interface

As seen in Fig. 7, the interface in front of a rotating detonation between (1) the fresh combustible gas layer and (2) the downstream gas burnt by the previous cycles has a rippled structure, which looks like Kelvin–Helmholtz instability. According to a simple calculation using the relation $U = (\rho_1 U_1 + \rho_2 U_2)/(\rho_1 + \rho_2) = (T_2 U_1 + T_1 U_2)/(T_1 + T_2)$, where U is the flowing velocity of K–H instability along the interface, the subscript 1 gives the quantities in the fresh combustible, and the subscript 2 the ones in the burnt gas, and using the observed values $T_1 = 300\,K$, $U_1 = 67.3\,m/s$, $T_2 = 1,100\,K$ and $U_2 = 395\,m/s$, U is given as $137.5\,m/s$, which is quite close to the observed value $112.3\,m/s$. Thus it is concluded that the K–H instability is the source of wavy interface structure.

4.8 Local explosion of an unburnt gas pocket generated by K–H ripple

The temperature and pressure fields during $t = 6169.8$–$6202.3\,\mu s$ given in Fig. 18a–c show the sequential behaviors of an unburnt gas pocket generated by K–H instability. Right at the junction point between the rotating detonation wavelet and ensuing oblique shock wave, a big unburnt gas pocket in Fig. 18a penetrates the wave front to create an unburnt gas pocket in Fig. 18b. In Fig. 18c it has clearly exploded to generate a dramatic blast wave strengthening and propagating into both detonation and oblique shock waves.

5 Specific impulse

Of high concern to engineers is the specific impulse given by rotating detonations. Figure 19 shows a behavior of the

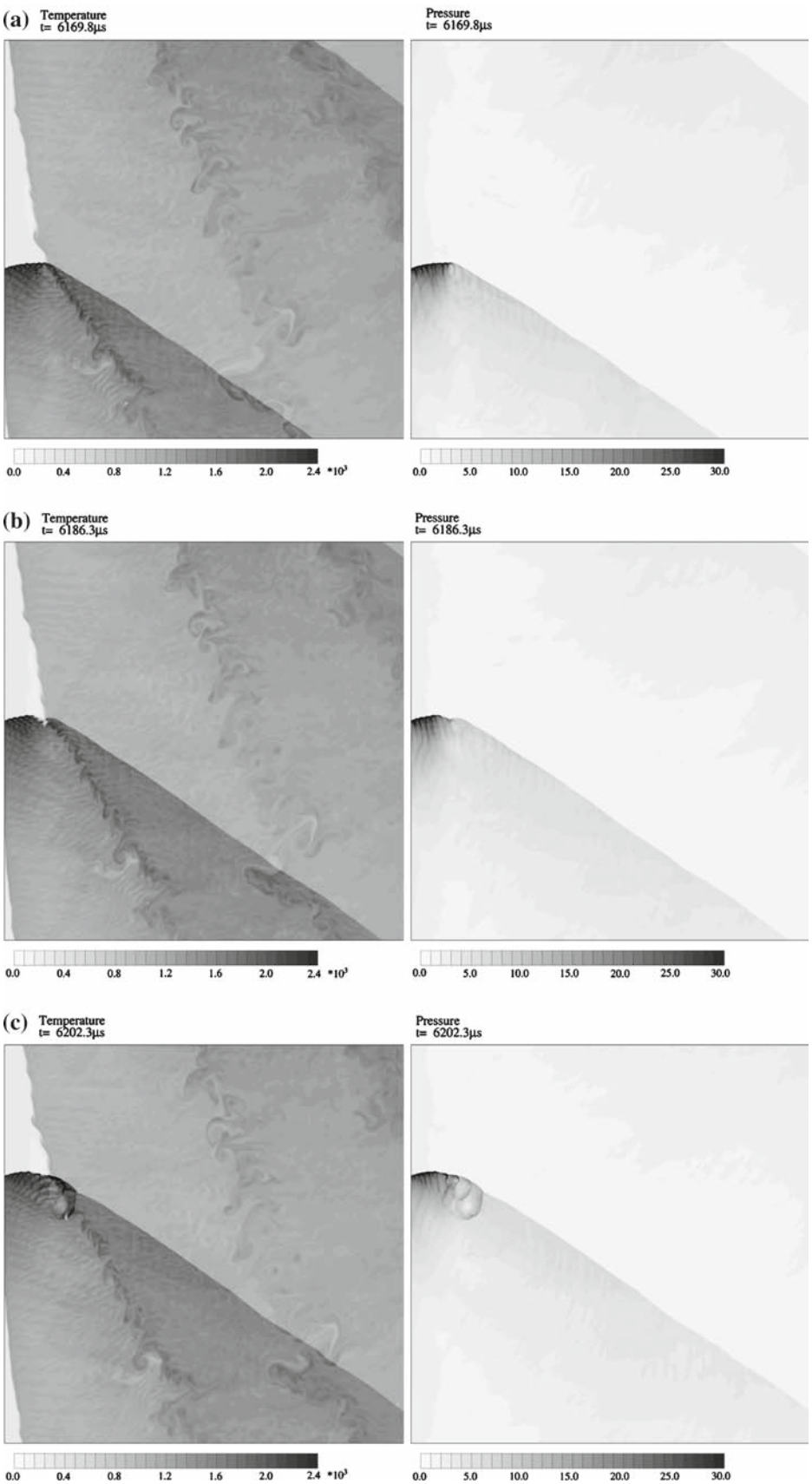

Fig. 18 Generation of an unburnt gas pocket explosion caused by K–H instability seen in temperature and pressure distributions at **a** $t = 6169.8$, **b** 6186.3 and **c** 6202.3 μs

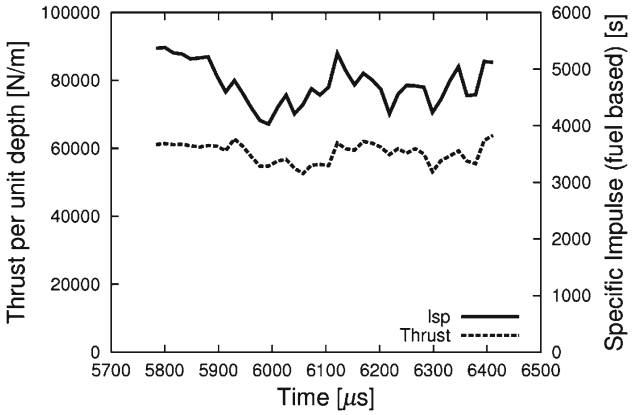

Fig. 19 Performance of RDE as thruster: Temporal variations of thrust per unit depth (60,000 N/m) and specific impulse (4,700 s)

thrust and specific impulse given by the present calculation. Accounting that the results after 6,100 μs are periodically converged ones, the fuel-based (for hydrogen in the mixture $2H_2 + O_2 + 7Ar$) specific impulse 4,700 s looks quite promising in comparison with other engines. Note, however, that the present calculation is based on Euler equations free from viscous losses, which in reality would discount the value 4,700 s.

6 Conclusion

A steadily propagating rotating detonation is established on a 2-dimensional simple chemistry flow model using a realistic injection condition, to give a number of interesting gasdynamic phenomena that can be applicable to the design of aerospace thrusters and power generators.

Since the present work is the first detailed analysis of rotating detonations, a number of new studies will be accomplished in future. Most importantly, the range of injection velocity that can stabilize rotating detonations has to be explored for a variety of detonable gas mixtures and their conditions. At least we want to report that increasing the injection velocity by 20%, the entire phenomena have not changed.

References

1. Nicholls, J.A., Wilkinson, H.R., Morrison, R.B.: Intermediate detonation as a thrust-producing mechanism. Jet Propuls. **27** (1957)
2. Voitsekhovskii, B.V.: Stationary detonation. Doklady USSR Acad. Sci. **129** (1959)
3. Voitsekhovskii, B.V., Mitrofanov, V.V., Topchiyan, M.E.: Structure of the detonation front in gases. Siberian Branch USSR Acad. Sci. Publ., Novosibirsk (1963)
4. Bykowski, F.A., Mitrofanov, V.V., Vedernikov, E.F.: Continuous detonation combustion of fuel–air mixtures, Combustion. Explos. Shock Waves **33**, 344–353 (1997). doi:10.1007/BF02671875
5. Bykovskii, F.A., Zhdan, S.A., Verdernikov, E.F.: Continuous spin detonation in ducted annular combustors. In: Roy, G., Frolov, S. (eds.) Application of Detonation to Propulsion, pp. 174–179. Torus press, Moscow (2004)
6. Wolanski, P., Kindracki, J., Fujiwara, T.: An experimental study of small rotating detonation engine. In: Roy, G, Frolov, S, Sinibaldi, J. (eds.) Pulsed and Continuous Detonations, pp. 332–338. Torus press, Moscow (2006)
7. Zhdan, S.A., Bykovskii, F.A., Vedernikov, E.F.: Mathematical modeling of a rotating detonation wave in a hydrogen-oxygen mixture, Combustion. Explos. Shock Waves **43**, 449–459 (2007). doi:10.1007/s10573-007-0061-y
8. Dabora, E.K., Nicholls, J.A., Morrison, R.B.: Tenth Symposium on Combustion, p. 817. Combustion Institute, Pittsburgh (1965)
9. Fujiwara, T., Tsuge, S.: Quasi-onedimensional analysis of gaseous free detonations. J. Phys. Soc. Jpn. **33**, 237–241 (1972). doi:10.1143/JPSJ.33.237
10. Tsuge, S., Fujiwara, T.: On the propagation velocity of a detonation-shock combined wave. Z. Angew. Math. Mech. **54**, 157–164 (1974). doi:10.1002/zamm.19740540305